nature astronomy

Article

https://doi.org/10.1038/s41550-024-02323-7

A constraint on the dissipative tidal deformability of neutron stars

Received: 12 January 2024

Accepted: 21 June 2024

Published online: 19 July 2024

Check for updates

Justin L. Ripley ✉, Abhishek Hegade K R ✉, Rohit S. Chandramouli & Nicolás Yunes

The gravitational waves emitted by neutron star binaries probe the physics of matter at supranuclear densities. During the late inspiral, tidal deformations raised on each star by the gravitational field of its companion depend crucially on the star's internal properties. The misalignment of a star's tidal bulge with its companion's gravitational field encodes the strength of internal dissipative processes, which imprint onto the phase of the gravitational waves emitted. Here, we analyse gravitational wave data from the GW170817 (binary neutron star) event detected by LIGO and Virgo and find a constraint on the dissipative tidal deformability of a neutron star. From this constraint, assuming a temperature profile for each star in the binary, we obtain an order of magnitude bound on the averaged bulk (ζ) and shear (η) viscosity of each star during the inspiral: $\zeta \lesssim 10^{31}\,\mathrm{g\,cm^{-1}\,s^{-1}}$ and $\eta \lesssim 10^{28}\,\mathrm{g\,cm^{-1}\,s^{-1}}$. We forecast that these bounds could be improved by two orders of magnitude with third-generation detectors, like Cosmic Explorer, using inspiral data. These constraints already inform nuclear physics models and motivate further theoretical work to better understand the interplay between viscosity and temperature in the late inspiral of neutron stars.

Neutron stars are the densest material objects in the Universe. Their interiors reach densities many times that of atomic nuclei at temperatures well below those probed by heavy-ion collisions. Determining the physical properties of neutron star matter, therefore, has remained an outstanding problem in astrophysics, gravitational physics and nuclear physics for almost a century[1]. Gravitational waves (GWs) from neutron star binaries encode the tidal deformations that neutron stars experience during their late inspiral before merger. These tidal deformations are in turn affected by the material properties of the stars. The prompt, conservative, relativistic, tidal response is described by the tidal deformability Λ (refs. 2–4), which encodes aspects of the equilibrium properties of neutron star matter through the neutron star equation of state (EOS)[1]. The GWs from the binary neutron star event GW170817 have been used to constrain the tidal deformability of these two neutron stars and, thus, their EOS[5,6].

The tidal response of a star can be visualized as a 'tidal bulge' that is sourced but not aligned with the time-varying, externally imposed, gravitational field of its companion (Fig. 1). Nonequilibrium dissipative effects within the star force the bulge to trail the orbit, inducing a tidal lag angle between the direction of the bulge and the orbital separation. The extent to which the tidal multipolar moments are misaligned with the external gravitational multipolar moments is, to a first approximation, described by the tidal lag time τ_{d}. The tidal lag time is a universal feature for self-gravitating astrophysical objects, from planets[7] to black holes[8,9], and it has been observed in many planetary systems[7,10]. This tidal misalignment torques the two stars and heats them up through tidal, viscous heating (for example, refs. 11,12).

Since the 1990s, it had been thought that the magnitude of these effects on the dynamics of neutron star binaries is too small to measure with GWs. Indeed, unphysically large values of viscosity are required to tidally lock the spins of the two stars to their orbit before merger[13]. Recent work in nuclear physics, however, suggests that weak-force processes can induce an effective bulk viscosity[14–16], which, although not large enough to tidally lock the spins of the two stars, may still have a measurable effect in the GWs emitted during the late inspiral[17]. This has motivated different numerical groups to model out-of-equilibrium

Illinois Center for Advanced Studies of the Universe & Department of Physics, University of Illinois at Urbana-Champaign, Urbana, IL, USA.
✉e-mail: lloydripley@gmail.com; ah30@illinois.edu

https://doi.org/10.1038/s41550-024-02323-7

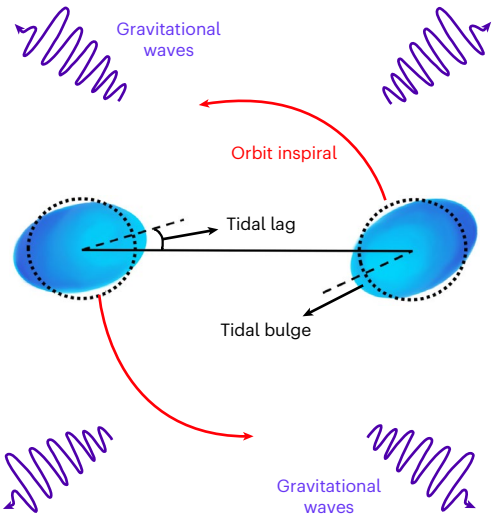

Fig. 1 | Illustration of the tidal responses of two stars in a quasi-circular binary (not to scale). Dissipative, out-of-equilibrium effects force the tidal bulge of each star to be misaligned with the gravitational field sourced by its companion.

effects during the late inspiral, merger and post-merger phases. Some groups have found bulk viscous effects to be enhanced during the late inspiral[15,18]. Moreover, other groups working with moment-based treatments of neutrino transport have not found evidence for the large out-of-thermodynamic-equilibrium effects necessary for producing an effective bulk viscosity during the late inspiral[19]. Nevertheless, these moment-based treatments of neutrino transport have revealed evidence of bulk viscous effects within a small window after the merger and before the matter returns to equilibrium[20]. Given these differences in the literature, it is crucial to utilize the available GW data to provide insights into out-of-equilibrium effects present during the late inspiral and merger phase.

Recently, the signature of the tidal lag in the GWs emitted by binary neutron star inspirals was reanalysed in ref. 17. Those authors found that this tidal lag was parametrically enhanced relative to that of conservative tidal effects. Conservative tidal effects first enter the GW phase proportional to ten powers of the orbital velocity relative to the leading-order term in a small-velocity, post-Newtonian (PN) expansion, which in the late inspiral is $v \approx (0.25\text{–}0.4)c$. Moreover, conservative effects are inversely proportional to five powers of the stellar compactness, that is, the dimensionless ratio of its mass to its radius, which for neutron stars is $C \approx 0.1\text{–}0.3$ (refs. 2,21). In contrast, dissipative tidal effects first enter the GW phase proportional to eight powers of the orbital velocity and inversely proportional to six powers of the stellar compactness[17]. Therefore, this parametric enhancement boosts the effect of dissipative tidal effects, making them potentially measurable with current ground-based GW detectors for physically plausible levels of dissipation within the stars.

The contribution of the tidal lag to the GW phase is captured by the dissipative counterpart to the conservative tidal deformability Λ: the dissipative tidal deformability Ξ, which can be mapped to the effective bulk and shear viscosities of the star[17,22]. Large values of bulk viscous dissipation could be sourced through Urca processes[14–16,23] or more exotic nuclear processes due to the presence of hyperons deep in the interior of a neutron star[24–27]. This effective viscosity depends on the particular nuclear and fluid models used, on the EOS of the star and on its temperature. Therefore, a measurement or constraint on Ξ cannot be translated to an independent measurement or constraint of any single one of these ingredients, without an assumption about the values of any two of the other quantities. Nonetheless, taking the expected values for these quantities, a preliminary forecast in ref. 17 suggested that the total extent of dissipative processes within neutron stars could be meaningfully constrained through an analysis of current GW data. Here, we carry out precisely such an analysis and constrain the dissipative tidal deformability of neutron stars using data from the GW170817 event detected by LIGO and Virgo[5].

GW model with dissipative tidal effects

We used the IMRPhenomPv2_NRTidal waveform model[28] for the detector response to the impinging GWs emitted in the inspiral of the binary neutron star system, which we enhanced to include tidal dissipation. Without tidal dissipation, the IMRPhenomPv2_NRTidal model depends on 17 parameters $\boldsymbol{\theta}_a$. These parameters, in addition to the non-tidal ones (such as the chirp mass $\mathcal{M} \equiv m_A^{3/5} m_B^{3/5}/M^{1/5}$ and the symmetric mass ratio $\eta_{sym} \equiv m_A m_B/M^2$, with $M \equiv m_A + m_B$ the total mass and $m_{A/B}$ the component masses), includes the tidal deformabilities of the stars $\Lambda_{A/B}$. In the frequency domain, we represent the model through the Fourier transform of the GW strain $\tilde{h}(f;\boldsymbol{\theta}) = A(f;\boldsymbol{\theta})\, e^{i\Psi(f;\boldsymbol{\theta})}$, where $A(f;\boldsymbol{\theta})$ is the Fourier GW amplitude and $\Psi(f;\boldsymbol{\theta})$ is the Fourier GW phase.

We enhanced the IMRPhenomPv2_NRTidal model by adding the leading PN contribution of the dissipative tidal deformability to the IMRPhenomPv2_NRTidal Fourier phase[17]:

$$\Psi(f;\boldsymbol{\theta}) = \Psi_{\mathrm{Pv2NRT}}(f;\boldsymbol{\theta}_a) - \frac{225}{4,096}\frac{1}{\eta_{sym}}\tilde{\Xi}\, u^3 \log(u), \qquad (1)$$

where $u \equiv (G\pi Mf/c^3)^{1/3}$ is effectively the orbital velocity. As the leading-order PN term in Ψ_{Pv2NRT} is proportional to u^{-5}, we see that the dissipative tidal contribution is of $\mathcal{O}(u^8)$ relative to the leading order, which is of $\mathcal{O}(u^2)$ larger than the $\mathcal{O}(u^{10})$ relative conservative tidal contribution in Ψ_{Pv2NRT}. The quantity $\tilde{\Xi}$ is the binary dissipative 'chirp' tidal deformability, which is a weighted sum of the dissipative tidal deformabilities of each star, $\Xi_{A,B}$:

$$\tilde{\Xi} \equiv 8\left(2\eta_{sym}^2 - 4\eta_{sym} + 1\right)\Xi_s - 8\sqrt{1-4\eta_{sym}}\left(1-2\eta_{sym}\right)\Xi_a, \qquad (2)$$

where $\Xi_s \equiv (\Xi_A + \Xi_B)/2$ and $\Xi_a \equiv (\Xi_A - \Xi_B)/2$. Therefore, the enhanced IMRPhenomPv2_NRTidal model contains 18 parameters: $\boldsymbol{\theta} = \boldsymbol{\theta}_a \cup \{\tilde{\Xi}\}$.

Constraint on dissipative tidal deformability from GW170817

As we discuss in more detail in Methods, we use a Bayesian parameter estimation to compute the posterior probability distribution for all the parameters of our enhanced IMRPhenomPv2_NRTidal GW model, given the publicly available 4 kHz GW170817 GW strain data[29]. Although we performed several checks of our analysis, here we describe only two separate analyses (we describe our other checks in Methods). In one run, we sampled the stars' individual conservative tidal deformabilities $\Lambda_{A,B}$, and in the other, we sampled the symmetric tidal deformability $\Lambda_s = (\Lambda_A + \Lambda_B)/2$, from which we found $\Lambda_a = (\Lambda_A - \Lambda_B)/2$ through the binary Love relations[30] (we marginalize over the uncertainty in those relations following ref. 31).

We present the binned, marginalized, posterior distribution on $\tilde{\Xi}$ from those two analyses in Fig. 2. We see that the data are informative, yielding a posterior that is noticeably different from the prior and peaking at zero with $\tilde{\Xi} < 1,200$ at 90% confidence. The posterior is additionally independent of whether or not we use the marginalized binary Love relations.

The marginalized posterior distributions for almost all other parameters are statistically consistent with those obtained by the LIGO–Virgo collaboration when one does not include dissipative tidal effects. The one exception is the posterior for $\tilde{\Lambda}$ (or equivalently for Λ_s or $\Lambda_{A,B}$), which is pushed to lower values due to correlations between the conservative and dissipative tidal deformabilities, as shown in Fig. 3. This implies that if the dissipative tidal deformability is present in the

https://doi.org/10.1038/s41550-024-02323-7

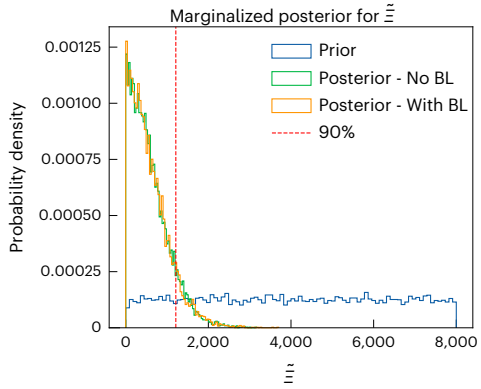

Fig. 2 | Marginalized posterior for the dissipative tidal deformability. The prior probability distribution for $\tilde{\Xi}$ is plotted in blue. The marginalized posterior for $\tilde{\Xi}$ is plotted in green (corresponding to sampling in $\Lambda_{A,B}$) and orange (corresponding to sampling in Λ_s). The 90% credible interval for the latter posterior is given by the vertical dashed line at $\tilde{\Xi} = 1,200$. Observe that the GW170817 data are sufficiently informative to constrain $\tilde{\Xi}$ compared to the prior, while remaining independent of the use of the binary Love relations[30,31]. No BL, without the marginalized binary Love relations; With BL, with the marginalized binary Love relations.

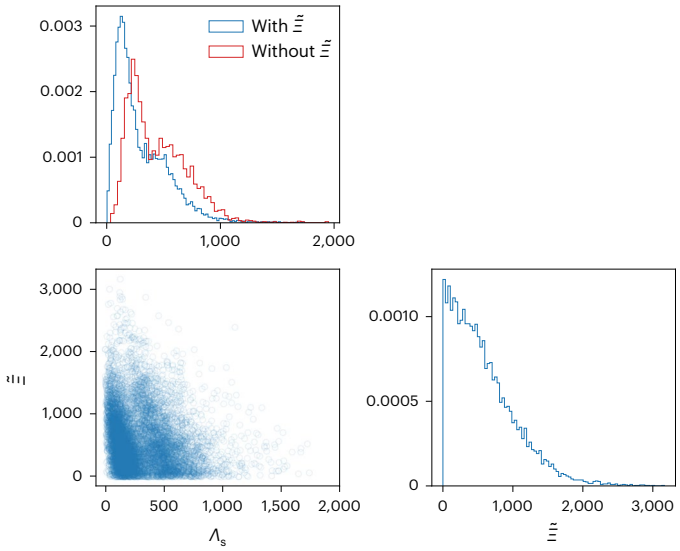

Fig. 3 | Corner subspace of the marginalized posterior distribution of Λ_s and $\tilde{\Xi}$. Shown in blue are the one-dimensional and two-dimensional marginalized posteriors on Λ_s and $\tilde{\Xi}$ corresponding to the analysis in which we did not use binary Love relations. Additionally shown in red in the top left panel is the one-dimensional marginalized posterior of Λ_s from the LIGO–Virgo analysis where $\tilde{\Xi}$ was not included (without binary Love relations). Observe that the two parameters are correlated. This correlation pushes the one-dimensional marginalized distribution of Λ_s to slightly lower values when including $\tilde{\Xi}$ in the analysis, compared to when we exclude the $\tilde{\Xi}$ correction (as is done in the LIGO–Virgo analysis of GW170817; ref. 6).

signal and that one neglects to incorporate its effects in the waveform model, then the estimate of the conservative tidal deformability will be biased to higher values than those contained in the signal.

Implications for nuclear physics

Any dissipative process within a neutron star adds cumulatively to the dissipative tidal deformability. As a consequence of this, an upper bound on $\tilde{\Xi}$ constrains the strength of any given dissipative process. Given a fluid model for the star, we can relate the dissipative tidal deformability to the tidal lag inside star A through[17]

$$\Xi_A = \frac{2}{3} k_{2,A} \left(\frac{1}{C_A{}^6}\right)\left(\frac{c\tau_{d,A}}{R_A}\right), \tag{3}$$

where $k_{2,A}$ is the conservative tidal Love number of the star, m_A and R_A are the stellar mass and radius, $C_A \equiv Gm_A/(R_A c^2)$ is its compactness and $\tau_{d,A}$ is its tidal lag time. We relate the tidal lag time to the viscosity through $\tau_{d,A} = p_{2,A}\langle\delta\rangle R_A c^2/(GM_A\langle e\rangle)$ (refs. 9,17), where $\langle\delta\rangle = \langle\eta\rangle$ (the shear viscosity) or $\langle\zeta\rangle$ (the bulk viscosity) depending on which source of dissipation is dominant. $p_{2,A}$ is a dimensionless constant that is computed for a given viscosity profile $\delta(e)$, and $\langle e\rangle$ is the average energy density. Using that the conservative tidal deformability $\Lambda_A \equiv (2k_{2,A}/3)/C_A^5$ (ref. 21), we then obtain

$$\begin{aligned}\Xi_A &= \frac{c^3}{G}\frac{p_{2,A}\Lambda_A}{C_A}\frac{\langle\delta\rangle}{\langle e\rangle m_A},\\ &\approx 26.1 \times \left(\frac{p_{2,A}}{0.01}\right)\left(\frac{\Lambda_A}{300}\right)\left(\frac{0.188}{C_A}\right)\left(\frac{\langle\delta\rangle}{10^{30}\,\mathrm{g\,cm^{-1}\,s^{-1}}}\right)\\ &\left(\frac{1.38\,M_\odot}{m_A}\right)\left(\frac{9\times10^{34}\,\mathrm{erg cm^{-3}}}{\langle e\rangle}\right).\end{aligned} \tag{4}$$

When bulk viscosity drives the process of dissipation, then $p_{2,A} \approx 0.01$, but it can be as high as $p_{2,A} \approx 5$ when shear viscosity dominates[22]. This is because gravitational fields cause a larger relative shearing motion than compression of the star[22].

We can map the constraint we obtained on the dissipative tidal deformability to the microphysics of dissipative processes inside a neutron star if we make the following assumptions. We assume that both stars in the binary had the same EOS and the same mass (which is consistent with the posterior for the GW170817 event). If so, they must also have the same compactness $C_A = C_B$. Furthermore, we assume that the stars have the same temperature profile and EOS, so that $\Lambda_A = \Lambda_B = \tilde{\Lambda}$ and $\Xi_A = \Xi_B = \tilde{\Xi}$. Inverting equation (4), we obtain

$$\begin{aligned}\langle\delta\rangle_A \approx 4.6\times10^{31}\,\frac{\mathrm{g}}{\mathrm{cm\,s}}\left(\frac{\tilde{\Xi}}{1,200}\right)\left(\frac{\langle e\rangle}{9\times10^{34}\,\mathrm{erg cm^{-3}}}\right)\\ \left(\frac{300}{\Lambda_A}\right)\left(\frac{0.01}{p_{2,A}}\right)\left(\frac{C_A}{0.188}\right)\left(\frac{m_A}{1.38\,M_\odot}\right).\end{aligned} \tag{5}$$

If shear viscosity was the dominant contribution to the dissipation, we would then obtain $\langle\eta\rangle \approx 9.15\times10^{28}\,\mathrm{g\,cm^{-1}\,s^{-1}}$ with a normalization factor of $(5/p_{2,A})$ instead of $(0.01/p_{2,A})$. Given our measured bound of $\tilde{\Xi} \lesssim 1,200$, we can place an upper bound on the averaged bulk and shear viscosity during the evolution of the GW170817 event. We, respectively, obtain $\langle\zeta\rangle_A \lesssim 4.57\times10^{31}\,\mathrm{g\,cm^{-1}\,s^{-1}}$ and $\langle\eta\rangle_A \lesssim 9.15\times10^{28}\,\mathrm{g\,cm^{-1}\,s^{-1}}$.

We now put this constraint into context by comparing it to current theoretical estimates of the viscosity of neutron stars. Viscosity generated by microscopic processes in neutron stars depends sensitively on the local stellar temperature profile T. Shear viscosity in neutron star cores scales as T^{-2} due to electron–muon scattering[32] and is expected to be less than $\langle\eta\rangle \lesssim 10^{22}\,\mathrm{g\,cm^{-1}\,s^{-1}}$. Shear viscous contributions due to the interface of a star's crust with its interior have been speculated to be as large as $\langle\eta\rangle \approx 10^{29}\,\mathrm{g\,cm^{-1}\,s^{-1}}$ (ref. 33). Bulk viscous contributions due to the presence of hyperons scale as T^{-2} and may be the dominant source of dissipation in neutron stars at very low (approximately kilo-electronvolt) temperatures, with the bulk viscosity predicted to exceed $\langle\zeta\rangle \approx 10^{30}\,\mathrm{g\,cm^{-1}\,s^{-1}}$ in some models[24–27]. As the binary enters the late inspiral, heating from tidal friction due to Urca reactions may increase the temperature of the two stars to tens of kilo-electronvolts[12]. Hyperonic bulk viscous contributions may heat the stars to higher temperatures[26]. Numerical relativity simulations of neutron star mergers suggest that tidal heating could increase the stellar temperature to a few mega-electronvolts during the last few orbits[34]. Bulk viscous contributions from direct and modified Urca

https://doi.org/10.1038/s41550-024-02323-7

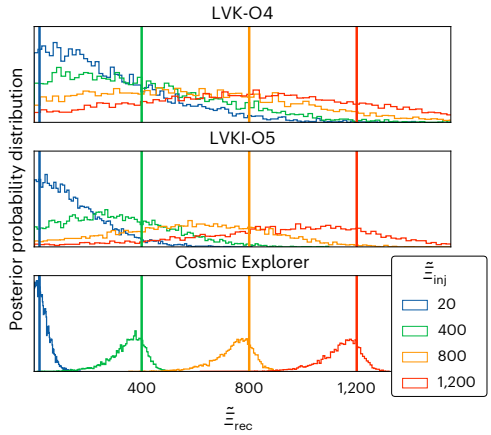

Fig. 4 | Histograms of the marginalized posterior distributions for $\tilde{\Xi}$ for zero-noise realizations of a GW170817-like event. The distributions were simulated as if detected with the O4 LIGO-Virgo-KAGRA (LVK-O4), O5 LIGO-Virgo-KAGRA-India (LVK-O5) and CE detector networks. The injected value of $\tilde{\Xi}$ is denoted by $\tilde{\Xi}_{inj}$ and the recovered value by $\tilde{\Xi}_{rec}$. The vertical lines represent the injected values of $\tilde{\Xi}$. We used the same uniform prior for $\tilde{\Xi}$ as described in the text.

processes are expected to dominate at high temperatures, as those reactions scale as T^4 and T^6, respectively[23]. Note that beyond a resonant peak, these reactions become weaker at higher temperatures. Current estimates place this peak at $T \approx 5$ MeV (ref. 35), higher than the temperatures expected to be reached by the stars during the inspiral. Typical predictions for the bulk viscosity for Urca-process-driven viscosity range from $\langle\zeta\rangle \approx 10^{26}$ g cm^{-1} s^{-1} when $T \approx 0.1$ MeV to $\langle\zeta\rangle \approx 10^{31}$ g cm^{-1} s^{-1} when $T \approx 1$ MeV, depending on the EOS[15,16].

In Methods, we estimate the number of GW cycles that $\tilde{\Xi}$ introduces in different regimes of the inspiral. We estimate that $\tilde{\Xi} \approx 1,200$ introduces ~1.86 GW cycles over the last ~27 orbits (corresponding roughly to orbital separations from ~83 km to contact), and a total of ~2.5 GW cycles over the entire inspiral. These results suggest that accounting for finite temperature and out-of-equilibrium effects during the last stage of the inspiral will be critical for mapping a constraint or detection of $\tilde{\Xi}$ to the underlying nuclear physics.

Future detectability of dissipative tides

We simulated synthetic GW detections for three different networks: ground-based detectors in the O4 and O5 era (the current LIGO observation run set-up and the following upgrade with the addition of the LIGO-India detector)[36], and the Cosmic Explorer (CE) era (one CE instrument at the current Hanford detector site)[37]. Each simulation consisted of 128 s of synthetic data, all starting at 40 Hz. The component masses and the symmetric conservative tidal deformabilities in each simulation were kept fixed at $m_{A,B} = 1.38\,M_\odot$ and $\Lambda_s = 584$, respectively, whereas the injected chirp dissipative tidal deformabilities were chosen to be $\tilde{\Xi} = \{20, 400, 800, 1200\}$. The choices for $m_{A,B}$ and Λ_s are consistent with the marginalized posterior distribution of these parameters in the GW170817 event, and the choice for $\tilde{\Xi}$ is consistent with the constraint we obtained at 90% confidence. As the luminosity distance was kept fixed, the signal-to-noise ratio (SNR) increased in the O4, O5 and CE simulations to ~60, ~100 and ~1,100, respectively.

We analysed these injections using Bayesian parameter estimation with our enhanced IMRPhenomPv2_NRTidal waveform model, following almost the same data analysis procedure as for the GW170817 event. The only difference is that we sampled only on $\{\mathcal{M}, q, \Lambda_s, \tilde{\Xi}\}$, and thus, we fixed all other parameters in the posterior to their injected values. We found empirically that this did not qualitatively affect our conclusions. We emphasize that we used the same uniform prior for $\tilde{\Xi}$ that we used in our analysis of GW170817. That is, we did not use our marginalized posterior for $\tilde{\Xi}_A$ from GW170817 as our prior for $\tilde{\Xi}$ in our injection runs.

Table 1 | MAP with the symmetric 90% credible interval about the MAP for each detector network and injected value of $\tilde{\Xi}$ (corresponding to the marginalized posteriors in Fig. 4)

$\tilde{\Xi}_{inj}$	$\tilde{\Xi}^{(O4)}_{MAP}$	$\tilde{\Xi}^{(O5)}_{MAP}$	$\tilde{\Xi}^{(CE)}_{MAP}$
20	89^{+522}_{-88}	16^{+301}_{-16}	11^{+57}_{-11}
400	197^{+615}_{-197}	270^{+301}_{-270}	380^{+116}_{-123}
800	528^{+560}_{-528}	584^{+451}_{-541}	771^{+132}_{-132}
1,200	803^{+704}_{-704}	974^{+584}_{-584}	$1{,}175^{+136}_{-145}$

The credible intervals are not symmetric about the MAP when one limit of the interval reaches a boundary of the posterior. We can translate a measurement on $\tilde{\Xi}$ to a measurement of the star's averaged viscosity using equation (5). These averaged viscosities are quoted in the abstract.

Figure 4 shows the marginalized posterior distribution for $\tilde{\Xi}$ for each injection. Notice that $\tilde{\Xi}$ is biased towards zero, which we attribute to correlations between $\tilde{\Xi}$ and the tidal deformability parameters $\Lambda_{A/B}$ (see Methods for more details). The one exception to this bias is the $\tilde{\Xi}_{inj} = 20$ injection for the O4 network. We attribute this increase to the fact that the spread in the posterior is very large for that network and that the injected value is close to zero (the lower bound of our prior). As expected, given the values of the SNR for the three detector networks, from Fig. 4 we see that the O5 network gives a modest improvement to the measurement of $\tilde{\Xi}$. For the O4 network, we see that the posterior is mostly supported away from zero only for the largest injected value of $\tilde{\Xi} = 1,200$, which lies at the 90% credible interval for our current measurement from GW170817 data. Table 1 shows the maximum of the posterior distribution (maximum a priori estimate (MAP)) for the marginalized distributions for $\tilde{\Xi}_{rec}$ along with the 90% symmetric credible interval about the MAP. With increasingly sensitive detectors (or, alternatively, with increasingly high SNR), the measurement of $\tilde{\Xi}$ simultaneously becomes less biased and more precise. This is consistent with our interpretation of the bias of $\tilde{\Xi}$ as arising from the correlation between $\tilde{\Xi}$ and $\Lambda_{A,B}$. With increasing SNR, these parameters simultaneously become less biased and can be measured more precisely.

Conclusions and outlook

Our analysis opens the door to a plethora of future work that will be required to extract precise inferences about out-of-equilibrium microphysics. First, one must find a way to break the degeneracy between the individual dissipative tidal deformabilities $\Xi_{A,B}$, which enter the GW phase through a linear combination encapsulated in $\tilde{\Xi}$. For the conservative tidal deformability $\tilde{\Lambda}$, this can be done with the binary Love relations[30,38] or by measuring the higher-order PN terms in the phase[39]. One should, thus, investigate the existence of similar, approximately universal relations for the dissipative tidal deformabilities and calculate the higher-order PN dissipative terms. Second, the effective bulk and shear viscosities of neutron stars are predicted to depend somewhat on the stars' EOS (for example, refs. 16,23–25,32,40). Mapping inferences on $\Xi_{A,B}$ to microphysics will, thus, require that one marginalize over all EOSs consistent with the data, including those with sharp features in the speed of sound (for example, refs. 41,42). Third, it will be critical to investigate systematic biases in parameter estimation that arise when dissipative tidal effects are not included and statistical biases in the measurement of $\tilde{\Xi}$ that arise due to the late inspiral being buried under detector noise. Finally, the bulk and shear viscosities of neutron stars also depend sensitively on their local temperature. Connecting the individual tidal deformabilities $\Xi_{A,B}$ to nuclear physics, therefore, requires knowledge of the temperature profiles within each star, which generally increase with time (and, thus, with GW frequency) in the late inspiral due to tidal friction[11,12]. This opens the possibility of learning not just about viscosity per se but also about the local temperature evolution and new aspects of the EOSs of neutron stars.

Methods

Data analysis methodology

We used Bayesian parameter estimation to compute the posterior probability distribution for all the parameters of our enhanced IMRPhenomPv2_NRTidal GW model, given 128 s of the publicly available 4 kHz GW170817 (glitch-cleaned) GW strain data[29]. We sampled over all 18 parameters of the model, and we marginalized over the reference phase. As usual in a GW data analysis, we assumed the noise to be Gaussian and stationary. The log-likelihood of the strain data $\tilde{s}(f)$ given a GW template $\tilde{h}(f;\boldsymbol{\theta})$ with model parameters $\boldsymbol{\theta}$ is then[43]

$$\ln \mathcal{L}(\tilde{s}|\boldsymbol{\theta}) = -\frac{1}{2}\left(\tilde{r}(\boldsymbol{\theta})|\tilde{r}(\boldsymbol{\theta})\right) = -2\int_0^\infty \mathrm{d}f \frac{|\tilde{r}(f;\boldsymbol{\theta})|^2}{S_n(f)}, \tag{6}$$

where $\tilde{r}(f;\boldsymbol{\theta}) \equiv \tilde{h}(f;\boldsymbol{\theta}) - \tilde{s}(f)$ is the residual signal and $S_n(f)$ is the noise power spectral density of the GW detector.

We used the Bilby GW library[44], modified to incorporate the dissipative tidal effects of equation (1), and sampled the likelihood with a nested sampling algorithm as implemented in DYNESTY (ref. 45). Within the Bilby interface to that code, we set nlive = 1,500, nact = 10, dlogz = 0.01, sample = 'rwalk' and bound = 'live'. As a consistency check on the c onvergence of our sampler to the true posterior distribution, we considered runs where nlive = 1,000, nact = 5 and dlogz = 0.1 and found that the posterior distribution did not noticeably change.

We chose the following priors for all our parameter estimatio n analyses. We set the chirp mass $\mathcal{M}$ to lie within the range $[1.184\,M_\odot, 1.25\,M_\odot]$, with a distribution that is equivalent to two uniform distributions over the component masses $M_{A,B}$. The mass ratio q lay within the range $[0.5,1]$ and was also sampled uniformly in the two component masses. As the IMRPhenomPv2_NRTidal model does not include spin corrections to the conservative tidal effects, we used the 'low-spin' prior defined in ref. 6. That is, we used uniform priors for the neutron star spins a_A and a_B over the range [0, 0.05]. Note that our dissipative tidal term contains no spin corrections either. When we sampled on the tidal deformabilities separately, we used a uniform prior over the interval $[0,3{,}000]$ for both deformabilities. When we sampled on the symmetric tidal deformability, we used a triangular prior with mean 1,500 and range $[0,3{,}000]$. For the dissipative tidal deformability $\tilde{\Xi}$, we chose a uniform prior in [0, 8,000]. Our lower prior on $\tilde{\Xi}$ was set to zero because we excluded the possibility of anti-dissipative processes within each star ($\Xi_A < 0$). The upper end of the prior on $\tilde{\Xi}$ was set by a heuristic constraint on the timescale for causal momentum transport across the star: dissipative and viscous effects should not transport momentum faster than light speed[13,17]. The rest of our waveform parameter priors followed those of ref. 6.

Validating our model and statistical analysis

To check our data analysis methodology, we sampled both independently in $\Lambda_{A,B}$ and by sampling the symmetric tidal deformability $\Lambda_s = (\Lambda_A + \Lambda_B)/2$, from which we found $\Lambda_a = (\Lambda_A - \Lambda_B)/2$ through the binary Love relations[30]. In the latter case, we marginalized over the uncertainty in the binary Love relations, following ref. 31. To quantify possible systematic sources of error from using a particular base waveform model, we considered two additional analyses for which we added the correction equation (1) to two different waveform models, IMRPhenomPv2_NRTidal (ref. 46) and IMRPhenomD_NRTidal (ref. 47). We found that the differences in the predictions for $\tilde{\Xi}$ for all three of these models (IMRPhnomPv2_NRTidal with and without the binary Love relations and IMRPhenomD_NRTidal with the binary Love relations) was too small to affect our analysis of GW170817 strain data.

We performed an additional check on our methods by performing the same parameter estimation procedure without $\tilde{\Xi}$ (that is by just using IMRPhenomPv2_NRTidal), which confirmed that our results were statistically consistent with the LIGO–Virgo analysis[6] of GW170817. Note that when we included $\tilde{\Xi}$ in our analysis, the marginalized posterior on Λ_s was pushed to slightly lower values compared to when $\tilde{\Xi}$ was excluded. We quantified the bias in the measurement of Λ_s by computing the difference between the maximum likelihood values of Λ_s obtained with and without $\tilde{\Xi}$. We found that $\Delta\Lambda_s^{\mathrm{ML}} = |\Lambda_s^{\mathrm{ML,with}\,\tilde{\Xi}} - \Lambda_s^{\mathrm{ML,without}\,\tilde{\Xi}}| \approx 46.78$. The half-widths of the 90% credible interval of the marginalized distribution of Λ_s in each case were $\delta_{\Lambda_s}^{\mathrm{with}\,\tilde{\Xi}} \approx 291.49$ and $\delta_{\Lambda_s}^{\mathrm{without}\,\tilde{\Xi}} \approx 381.00$. To conclude, the bias in the maximum likelihood of Λ_s is contained within both estimates of the statistical error.

We see from the bottom left panel of Fig. 3 that the correlation between Λ_s and $\tilde{\Xi}$ is the reason for the shift of the marginalized posterior on Λ_s. That is, our agnostic analysis performed by including both conservative and dissipative tides resulted in slightly tighter constraints on the maximum value of the conservative tides Λ_A and Λ_B than was obtained by the LIGO–Virgo analysis.

Finally, we performed another consistency check of our result for the posterior probability distribution for $\tilde{\Xi}$, shown in Fig. 2, by considering different prior distributions for $\tilde{\Xi}$. We used a uniform prior in $\Xi_{A/B}$ to obtain the prior on $\tilde{\Xi}$. We also sampled using a log-uniform prior on $\tilde{\Xi}$. In both these cases, we found that when we divided the posterior probability distribution, multiplied by our flat prior for $\tilde{\Xi}$ and renormalized, we obtained a distribution statistically consistent with that shown in Fig. 2.

Estimating the impact of the tidal terms

To estimate the frequency and radius at which tidal effects start to appreciably affect the phase of emitted GWs and as another check on the robustness of our analysis, here we compare the leading-order phase contributions of the adiabatic and dissipative tides to the leading phase of a Newtonian binary of point particles. In particular, we computed the fraction p of the tidal phase with respect to the Newtonian phase for both the conservative and dissipative tidal effects. We took the fiducial value of $p = 0.025$. The leading-order phase contribution for $\tilde{\Xi}$ is given in equation (1). Recall that the leading-order phasing contribution of $\tilde{\Lambda}$ is[21]

$$\Delta\Psi_\Lambda = -\frac{117}{256}\frac{\tilde{\Lambda}}{\eta_{\mathrm{sym}}}u^5, \tag{7}$$

whereas the leading-order phase contribution for a Newtonian binary of point particles is (for a review, see, for example, ref. 43)

$$\Psi_{\mathrm{pp}} = \frac{3}{128}\frac{1}{\eta_{\mathrm{sym}}}u^{-5}. \tag{8}$$

Setting $\Delta\Psi_\Lambda/\Psi_{\mathrm{pp}} = p$ and solving for the GW frequency f (or the orbital radius r, using the relation $u^2 = GM/(rc^2)$), we obtained

$$\begin{aligned} f &\approx 467\,\mathrm{Hz}\left(\frac{m}{2.8\,M_\odot}\right)^{-1}\left(\frac{p}{0.025}\right)^{3/10}\left(\frac{\tilde{\Lambda}}{575}\right)^{-3/10}, \\ r &\approx 55\,\mathrm{km}\left(\frac{m}{2.8\,M_\odot}\right)\left(\frac{p}{0.025}\right)^{-1/5}\left(\frac{\tilde{\Lambda}}{575}\right)^{1/5}. \end{aligned} \tag{9}$$

For the dissipative tidal effect, setting $|\Delta\Psi_{\tilde{\Xi}}/\Psi_{\mathrm{pp}}| = p$, we solved the resulting transcendental equation numerically for f (or r),

$$-\frac{75}{32}\tilde{\Xi}u^8\log u = p. \tag{10}$$

Setting $p = 0.025$, $\tilde{\Xi} = 1,200$ (based on the constraint from GW170817) and $m = 2.8\,M_\odot$, we found $f \approx 253$ Hz and $r \approx 84\,\mathrm{km} \approx 8R_A$. In other words, dissipative tidal effects typically become important at an earlier stage of the inspiral than conservative tidal effects. Note that for a fixed fraction p, a larger (smaller) $\tilde{\Xi}$ will contribute more at a lower (higher) frequency. That is, the tidal effects grow stronger as the two stars in the

binary move faster. When we set $\tilde{\Xi} = 1,200$, from $f \approx 253$ Hz until $f \approx 1{,}569$ Hz (corresponding to the last stable orbit for an $m = 2.8M_{\odot}$ mass binary), $\Delta\Psi_{\tilde{\Xi}}$ accumulated 1.86 GW cycles (equation (1)). For reference, over the entire inspiral (from 10 to 1,569 Hz), $\Delta\Psi_{\tilde{\Xi}}$ contributed 2.5 GW cycles whereas $\Psi_{\rm pp}$ contributed ~6,060 GW cycles. In conclusion, most of the contribution from $\tilde{\Xi}$ was accumulated during the late stage of binary inspiral.

Data availability

All relevant data that supports the findings of this study, including the scripts we used to produce the figures in the article, are available via Zenodo at https://doi.org/10.5281/zenodo.11626502 (ref. 48).

Code availability

The code we used to perform our analysis is available via Zenodo at https://doi.org/10.5281/zenodo.11589416 (ref. 49).

References

1. Burgio, G. F., Schulze, H. J., Vidana, I. & Wei, J. B. Neutron stars and the nuclear equation of state. *Prog. Part. Nucl. Phys.* **120**, 103879 (2021).
2. Hinderer, T. Tidal Love numbers of neutron stars. *Astrophys. J.* **677**, 1216–1220 (2008).
3. Damour, T. & Nagar, A. Relativistic tidal properties of neutron stars. *Phys. Rev. D* **80**, 084035 (2009).
4. Binnington, T. & Poisson, E. Relativistic theory of tidal Love numbers. *Phys. Rev. D* **80**, 084018 (2009).
5. Abbott, B. P. et al. GW170817: observation of gravitational waves from a binary neutron star inspiral. *Phys. Rev. Lett.* **119**, 161101 (2017).
6. Abbott, B. P. et al. Properties of the binary neutron star merger GW170817. *Phys. Rev. X* **9**, 011001 (2019).
7. Ogilvie, G. I. Tidal dissipation in stars and giant planets. *Annu. Rev. Astron. Astrophys.* **52**, 171–210 (2014).
8. Hartle, J. B. Tidal friction in slowly rotating black holes. *Phys. Rev. D* **8**, 1010–1024 (1973).
9. Poisson, E. Tidal interaction of black holes and Newtonian viscous bodies. *Phys. Rev. D* **80**, 064029 (2009).
10. Zahn, J.-P. Tidal dissipation in binary systems. *EAS Publ. Ser.* **29**, 67–90 (2008).
11. Lai, D. Resonant oscillations and tidal heating in coalescing binary neutron stars. *Mon. Not. R. Astron. Soc.* **270**, 611–629 (1994).
12. Arras, P. & Weinberg, N. N. Urca reactions during neutron star inspiral. *Mon. Not. R. Astron. Soc.* **486**, 1424–1436 (2019).
13. Bildsten, L. & Cutler, C. Tidal interactions of inspiraling compact binaries. *Astrophys. J.* **400**, 175–180 (1992).
14. Alford, M. G. & Harris, S. P. Damping of density oscillations in neutrino-transparent nuclear matter. *Phys. Rev. C* **100**, 035803 (2019).
15. Most, E. R. et al. Projecting the likely importance of weak-interaction-driven bulk viscosity in neutron star mergers. *Mon. Not. R. Astron. Soc.* **509**, 1096–1108 (2021).
16. Yang, Y., Hippert, M., Speranza, E. & Noronha, J. Far-from-equilibrium bulk-viscous transport coefficients in neutron star mergers. *Phys. Rev. C* **109**, 015805 (2024).
17. Ripley, J. L., Hegade K. R., A. & Yunes, N. Probing internal dissipative processes of neutron stars with gravitational waves during the inspiral of neutron star binaries. *Phys. Rev. D* **108**, 103037 (2023).
18. Chabanov, M. & Rezzolla, L. Impact of bulk viscosity on the post-merger gravitational-wave signal from merging neutron stars. Preprint at https://arxiv.org/abs/2307.10464 (2023).
19. Radice, D., Bernuzzi, S., Perego, A. & Haas, R. A new moment-based general-relativistic neutrino-radiation transport code: methods and first applications to neutron star mergers. *Mon. Not. R. Astron. Soc.* **512**, 1499–1521 (2022).
20. Espino, P. L. et al. Neutrino trapping and out-of-equilibrium effects in binary neutron star merger remnants. *Phys. Rev. Lett.* **132**, 211001 (2024).
21. Flanagan, E. E. & Hinderer, T. Constraining neutron star tidal Love numbers with gravitational wave detectors. *Phys. Rev. D* **77**, 021502 (2008).
22. Hegade K. R., A., Ripley, J. L. & Yunes, N. Dynamical tidal response of nonrotating relativistic stars. *Phys. Rev. D* **109**, 104064 (2024).
23. Sawyer, R. F. Bulk viscosity of hot neutron-star matter and the maximum rotation rates of neutron stars. *Phys. Rev. D* **39**, 3804–3806 (1989).
24. Jones, P. B. Bulk viscosity of neutron star matter. *Phys. Rev. D* **64**, 084003 (2001).
25. Lindblom, L. & Owen, B. J. Effect of hyperon bulk viscosity on neutron star R modes. *Phys. Rev. D* **65**, 063006 (2002).
26. Alford, M. G. & Haber, A. Strangeness-changing rates and hyperonic bulk viscosity in neutron star mergers. *Phys. Rev. C* **103**, 045810 (2021).
27. Gusakov, M. E. & Kantor, E. M. Bulk viscosity of superfluid hyperon stars. *Phys. Rev. D* **78**, 083006 (2008).
28. Dietrich, T. et al. Improving the NRTidal model for binary neutron star systems. *Phys. Rev. D* **100**, 044003 (2019).
29. Abbott, R. et al. Open data from the first and second observing runs of Advanced LIGO and Advanced Virgo. *SoftwareX* **13**, 100658 (2021).
30. Yagi, K. & Yunes, N. Binary Love relations. *Class. Quantum Gravity* **33**, 13LT01 (2016).
31. Carson, Z., Chatziioannou, K., Haster, C.-J., Yagi, K. & Yunes, N. Equation-of-state insensitive relations after GW170817. *Phys. Rev. D* **99**, 083016 (2019).
32. Shternin, P. S. & Yakovlev, D. G. Shear viscosity in neutron star cores. *Phys. Rev. D* **78**, 063006 (2008).
33. Kochanek, C. S. Coalescing binary neutron stars. *Astrophys. J.* **398**, 234–247 (1992).
34. Perego, A., Bernuzzi, S. & Radice, D. Thermodynamics conditions of matter in neutron star mergers. *Eur. Phys. J. A* **55**, 124 (2019).
35. Alford, M. G., Haber, A. & Zhang, Z. Isospin equilibration in neutron star mergers. *Phys. Rev. C* **109**, 055803 (2024).
36. Abbott, B. P. et al. Prospects for observing and localizing gravitational-wave transients with Advanced LIGO, Advanced Virgo and KAGRA. *Living Rev. Relativ.* **21**, 3 (2018).
37. Abbott, B. P. et al. Exploring the sensitivity of next generation gravitational wave detectors. *Class. Quantum Gravity* **34**, 044001 (2017).
38. Yagi, K. & Yunes, N. Approximate universal relations among tidal parameters for neutron star binaries. *Class. Quantum Gravity* **34**, 015006 (2017).
39. Vines, J., Flanagan, E. E. & Hinderer, T. Post-1-Newtonian tidal effects in the gravitational waveform from binary inspirals. *Phys. Rev. D* **83**, 084051 (2011).
40. Haensel, P., Levenfish, K. P. & Yakovlev, D. G. Bulk viscosity in superfluid neutron star cores. I. Direct Urca processes in NPE μ matter. *Astron. Astrophys.* **357**, 1157–1169 (2000).
41. Tan, H., Dexheimer, V., Noronha-Hostler, J. & Yunes, N. Finding structure in the speed of sound of supranuclear matter from binary Love relations. *Phys. Rev. Lett.* **128**, 161101 (2022).
42. Tan, H., Dore, T., Dexheimer, V., Noronha-Hostler, J. & Yunes, N. Extreme matter meets extreme gravity: ultraheavy neutron stars with phase transitions. *Phys. Rev. D* **105**, 023018 (2022).
43. Maggiore, M. *Gravitational Waves. Vol. 1. Theory and Experiments* (Oxford Univ. Press, 2007).

44. Ashton, G. et al. BILBY: a user-friendly Bayesian inference library for gravitational-wave astronomy. *Astrophys. J. Suppl. Ser.* **241**, 27 (2019).
45. Speagle, J. S. DYNESTY: a dynamic nested sampling package for estimating Bayesian posteriors and evidences. *Mon. Not. R. Astron. Soc.* **493**, 3132–3158 (2020).
46. Dietrich, T. et al. Matter imprints in waveform models for neutron star binaries: tidal and self-spin effects. *Phys. Rev. D* **99**, 024029 (2019).
47. Dietrich, T., Bernuzzi, S. & Tichy, W. Closed-form tidal approximants for binary neutron star gravitational waveforms constructed from high-resolution numerical relativity simulations. *Phys. Rev. D* **96**, 121501 (2017).
48. Ripley, J. et al. Data+analysis+plotting scripts for 'Constraint on the dissipative tidal deformability of neutron stars'. *Zenodo* https://doi.org/10.5281/zenodo.11626502 (2024).
49. Ripley, J. et al. JLRipley314/NRTidal-D: code used in 2312.11659. *Zenodo* https://doi.org/10.5281/zenodo.11589416 (2024).

Acknowledgements

We would like to thank J. Noronha, J. Noronha-Hostler, C. Talbot, Y. Yang, M. Hippert and M. Alford for helpful discussions. We acknowledge support from the National Science Foundation through award PHY-2207650 (J.L.R., A.H. and N.Y.) and from the University of Illinois Graduate College Dissertation Completion Fellowship (R.C.). We also acknowledge the Illinois Campus Cluster Program, the Center for Astrophysical Surveys and the National Center for Supercomputing Applications for the computational resources that were used to produce the results of our paper.

Author contributions

J.L.R., R.S.C. and A.H.K.R. performed the data analysis. All authors contributed to the writing of the manuscript and to the interpretation of the results.

Competing interests

The authors declare no competing interests.

Additional information

Correspondence and requests for materials should be addressed to Justin L. Ripley or Abhishek Hegade K R.

Peer review information *Nature Astronomy* thanks the anonymous reviewers for their contribution to the peer review of this work.